APPLIED MATERIALS AND TECHNOLOGY

Jamt.ejournal.unri.ac.id

Research Article

Powder metallurgy synthesis of Pd-doped MoS_2: A structural and morphological study

Jonas Miguel Nogueira*, Adhimar Flavio Oliveira, Rero Marques Rubinger, Celso Henrique Correa Carvalho

ABSTRACT: This study reports the synthesis and structural characterization of palladium (Pd)-doped molybdenum disulfide (MoS_2) produced via the powder metallurgy route. The primary objective was to investigate how Pd incorporation influences the structural, morphological, and electrical properties of MoS_2, thereby demonstrating the advantages of powder metallurgy compared to conventional synthesis techniques. The materials were analyzed by X-ray diffraction (XRD), scanning electron microscopy (SEM) coupled with energy-dispersive spectroscopy (EDS), Fourier-transform infrared spectroscopy (FTIR), and Raman spectroscopy. XRD confirmed the retention of the hexagonal MoS_2 phase without the formation of secondary Pd-related phases, indicating successful substitutional doping. SEM–EDS analyses revealed a uniform Pd distribution and progressive morphological evolution with increasing Pd content, characterized by enhanced surface roughness and improved particle dispersion. FTIR and Raman spectra showed modifications in bonding environments and vibrational modes, evidencing the structural influence of Pd atoms on the MoS_2 lattice. Electrical measurements, performed using both I–V and four-point probe methods, demonstrated a conductivity increase from 9.6 $\times 10^{-9}$ S·m^{-1} for pure MoS_2 to 1.6 $\times 10^{-5}$ S·m^{-1} and 1.9 $\times 10^{-5}$ S·m^{-1} for the 1% and 2% Pd-doped samples, respectively. This enhancement is attributed to the higher charge carrier density and improved interlayer charge transport induced by Pd doping. These findings confirm that powder metallurgy provides an effective and scalable synthesis pathway for achieving homogeneous Pd incorporation in MoS_2. The resulting materials exhibit excellent structural integrity and enhanced electrical performance, making them promising candidates for catalytic, sensing, and energy storage applications.

Keywords: *Transition metal dichalcogenides, Substitutional doping, Electrical Conductivity, Structural characterization, Energy and sensing application*

1. INTRODUCTION

The escalating demand for high-efficiency sensors and energy systems, with a particular focus on energy storage and electronic devices, has intensified in recent years [1,2]. Driven by a growing emphasis on sustainability, enhancing the performance of these devices has become a critical research priority. Energy storage devices, such as batteries and supercapacitors, are integral for integrating renewable energy sources and advancing electric mobility [3]. Similarly, highly sensitive sensors and efficient catalysts are crucial for environmental monitoring and industrial chemical processes.

The performance of these technologies is intrinsically linked to the fundamental properties of the semiconductor materials employed in their fabrication [4]. Consequently, research focused on discovering and refining semiconductor materials is paramount for achieving significant technological advancements in these areas [5, 6]. In this context, the two-dimensional transition metal dichalcogenide Molybdenum Disulfide (MoS_2) has emerged as a particularly promising candidate. It exhib-

OPEN ACCESS

Affiliation
Universidade Federal de Itajubá, Av BPS, 1303, Itajubá, 37500-903, Brasil

***Correspondence**
Email: jonasmigueln@unifei.edu.br

ORCID
Nogueira, J., M.: 0009-0000-1913-682X
Oliveira, A., F.: 0000-0003-2586-7359
Rubinger, R., M.: 0000-0003-1718-9658
Carvalho, C., H., C.: 0000-0001-7667-6961

Received: October 01, 2025
Revised: October 16, 2025
Accepted: October 25, 2025

How to cite: Nogueira, J., M., Oliveira, A., F., N., Rubinger, R., M., Carvalho., C., H., C., (2025). Powder Metallurgy Synthesis of Pd-Doped MoS_2: A Structural and Morphological Study. *Journal of Applied Materials and Technology*, 7(1), 31–40. https://doi.org/10.31258/Jamt.7.1.31-40.

its a unique combination of advantageous properties, including a suitable electronic bandgap, high carrier mobility, excellent physicochemical stability, and a layered atomic structure amenable to nanoscale device integration [5, 6].

A promising strategy to augment the intrinsic properties of MoS_2 is doping with transition metals such as Palladium (Pd). As a dopant, palladium is recognized for its exceptional catalytic activity and electronic characteristics. The introduction of Pd atoms into the MoS_2 lattice can significantly enhance electrical conductivity and modulate the electronic structure, thereby boosting the material's performance and responsiveness in various applications [7–9]. This substitutional doping strategy not only creates new avenues in materials engineering but also holds considerable potential for developing next-generation devices, including highly sensitive sensors, efficient catalysts for chemical reactions, and components for energy storage [7, 8, 10].

While various techniques can be employed for doping MoS_2, conventional methods such as chemical vapor deposition (CVD), sputtering, and sol-gel synthesis present notable drawbacks. CVD is often hindered by process complexity and scalability issues [11], sputtering can lead to nonuniform dopant distribution and inconsistent electrical properties [12], and sol-gel methods can be slow and result in disordered porosity and potential impurities [13]. In contrast, powder metallurgy offers superior control over composition and microstructure, yielding highly uniform, doped materials crucial for high-performance applications [14–18]. This approach allows for the homogeneous mixing of precursor particles, followed by a sintering process that promotes robust interaction between the materials, making it especially suitable for fabricating high-quality nanoscale devices.

The functionalization of MoS_2 via Palladium (Pd) doping represents a promising strategy to enhance its material properties [10]. Palladium's viability as a substitutional dopant is supported by its physicochemical compatibility with the MoS_2 lattice, including a minimal atomic radius mismatch (3.60%) and analogous electronegativity and valence states [7, 8]. This atomic-level modification is expected to create active catalytic sites for processes such as the oxygen evolution reaction (OER) and improve electronic transport, modulating the electronic structure through covalent Pd-S bond formation to enhance performance in sensor and energy applications [19–21].

In light of these considerations, this work reports on the synthesis and structural characterization of Pd-doped MoS_2 using a powder metallurgy approach. We provide a systematic investigation to elucidate the effects of palladium doping and to establish a foundation for its future use in next-generation devices such as sensors and catalysts.

Despite extensive research on Pd-doped MoS_2 synthesized through chemical vapor deposition, sol–gel, and hydrothermal routes, there remains a lack of systematic investigation into the structural and electrical effects of Pd incorporation in MoS_2 prepared via powder metallurgy. This study addresses that gap by demonstrating powder metallurgy as a controllable and scalable alternative synthesis route capable of producing homogeneously doped 2D materials with tunable microstructural and electronic properties.

In contrast to previous studies employing chemical vapor deposition, sputtering, or sol–gel techniques, which often face challenges related to dopant uniformity, defect control, and scalability, this work introduces the powder metallurgy route as an alternative synthesis method for Pd-doped MoS_2.

To the best of our knowledge, this study represents the first successful application of powder metallurgy for the synthesis of Pd-doped MoS_2, demonstrating its ability to achieve homogeneous Pd incorporation within the MoS_2 lattice without the formation of secondary Pd-based phases. The combination of XRD, SEM–EDS, and Raman analyses confirmed the structural integrity of the hexagonal MoS_2 phase and the effective substitutional doping of Pd atoms.

Moreover, the samples produced through this route exhibited a three-order-of-magnitude enhancement in electrical conductivity compared to undoped MoS_2, directly evidencing the influence of Pd on charge carrier generation and interlayer transport. These findings highlight not only the effectiveness of the powder metallurgy process in tailoring the microstructure and electronic properties of MoS_2, but also its potential as a scalable, compositionally controlled technique for fabricating doped 2D materials suitable for catalytic, sensing, and energy storage applications.

2. EXPERIMENTAL

The synthesis involved three primary raw materials. MoS_2 powder, with a purity of >98wt%. and a particle size distribution of 0.5μm to 10μm, was obtained as a donation from Ferroligas Nu´cleo. The palladium source was Palladium(II) Acetylacetonate, a yellow powder with 99.9wt.% purity. Additionally, elemental sulfur (S), in the form of a yellow powder with a purity of >99.5wt.%, was sourced from Exodo Cient´ıfica.ˆ

The phases of the experimental procedure adopted for this work are detailed in the flowchart in Figure 1.

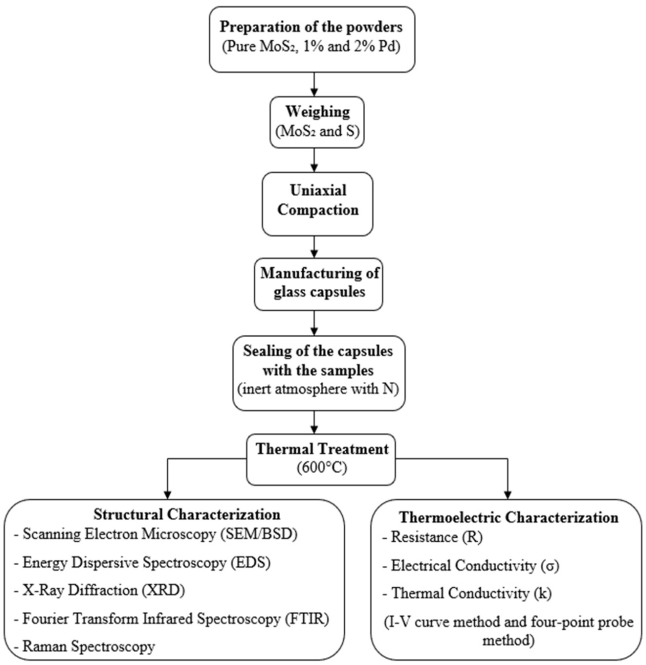

Figure 1. Flowchart of the experimental procedure steps.

Table 1. Masses in grams for the pure and doped MoS_2 compositions.

Sample	Mass (g)
Pure MoS_2	2.500
MoS_2 – 1% Pd	2.525
MoS_2 – 2% Pd	2.550

The samples were divided into pure MoS_2, MoS_2 with 1% Pd, and MoS_2 with 2% Pd. The powders were weighed on a SHIMADZU model AUW220D analytical balance and mixed using a mortar and pestle. Table 1 shows the final mass for each composition based on a 2.5g starting mass of MoS_2.

For the compaction process, a cylindrical die with an internal diameter of 14mm was utilized. Each die was charged with 0.5g of powder and subsequently subjected to uniaxial pressing in a SKAY hydraulic press. A load of 1t was applied and maintained for a duration of 5min, after which the resulting specimen was ejected. A total of nine specimens were prepared in triplicate for three distinct compositions: undoped MoS_2, MoS_2 doped with 1% Pd, and MoS_2 doped with 2% Pd. Additionally, a discrete sulfur pellet was pressed for each compositional set and cosealed with the specimens in silicate glass tubes to maintain a sulfur-rich atmosphere during the subsequent heat treatment. This was intended to keep the MoS_2 structure intact, as it readily reacts with oxygen at high temperatures to form MoO_3.

Before heat treatment, the compacted specimens were sealed in silicate glass ampoules. For each composition, three specimens and one supplementary sulfur pellet were placed in an ampoule, which was then evacuated and subsequently backfilled with nitrogen gas to establish an inert atmosphere. The heat treatment was conducted in a JUNG model 2312 furnace, where the sealed ampoules were subjected to a thermal profile consisting of heating to 600°C, holding for a 2h dwell time, and passive cooling inside the furnace.

For XRD, the powder sample was analyzed using a PANalytical model X'Pert Pro. The test parameters were: measurement time of 1s per step, step size of 0.02°, 2θ scan range from 5° to 90°, using a copper tube (Cu–Kα, λ = 0.1542nm), with a voltage of 40kV and a current of 30mA.

The morphology and elemental composition of the bulk specimens were investigated by SEM coupled with EDS, using a Carl Zeiss EVO MA15 instrument. The analyses were performed with an accelerating voltage (EHT) of 15.00kV and a working distance ranging from 8.0mm to 9.5mm. Surface topography was imaged using the secondary electron detector, while compositional contrast was visualized with the backscattered electron detector. To ensure representative results, micrographs were acquired at a magnification of 5000x from at least three distinct regions on each specimen, with concurrent EDS providing the elemental analysis.

FTIR spectroscopy was performed on the bulk specimens using a PerkinElmer Spectrum 100 instrument. Spectra were recorded in transmittance mode over a wavenumber range of 4000cm^{-1} to 600cm^{-1}. Each fnal spectrum was an average of 12 scans acquired over a total duration of one minute.

Raman spectra of the specimens were acquired using a labRAM HR Evolution system equipped with a Syncerity OE detector. The analysis was conducted using a 532nm laser excitation source through a 50x objective lens. Each spectrum represents the accumulation of 20 scans, with an integration time of 10s per scan, over the spectral range of 100cm^{-1} to 1400cm^{-1}.

The electrical resistance (R) was first determined by I-V curve analysis using a Keithley 2612A SourceMeter. A custom Python script automated a voltage sweep from −10V to 10V in 0.05V increments, recording the resultant current at each point. R was then calculated from the linear regression of the I-V curve.

3. RESULT AND DISCUSSION

3.1. Structural characterizations. The pressed specimens exhibited sufficient green strength, allowing them to be handled without damage. The samples presented a satisfactory surface finish with a metallic luster, which was particularly noticeable after the addition of Pd. Figure 2 shows a representative specimen before and after the heat treatment process. After cooling, the silicate glass tubes were broken, and the specimens were retrieved for structural characterization. To obtain information on the composition and general structural properties, SEM was performed in BSD mode on the MoS_2, MoS_2–1%Pd, and MoS_2–2% samples heat-treated at 600°C. The resulting micrographs, taken at 5000x magnification, are shown in Figure 3.

The micrograph of pure MoS_2 (Figure 3a) reveals a characteristic stacked-layer structure, typical of lamellar materials. The surface displays a relatively homogeneous morphology with some aggregated regions, indicating that the MoS_2 maintained its crystalline structure after the heat treatment [22]. Upon analyzing the micrograph of the MoS_2 with 1% Pd (Figure 3b), a slight alteration in morphology is perceptible. Small particles can be observed dispersed on the MoS_2 matrix, suggesting the presence of Pd nanoparticles. The structure also appears rougher and more fragmented, which may indicate an interaction between palladium and MoS_2, an exfoliation of the layers. In the micrograph of the sample with 2% Pd (Figure 3c), the differences become even more evident. The presence of well-distributed particles on the surface is more intense, suggesting an increased concentration of palladium. Furthermore, greater agglomeration and possible grain growth are observed, indicating that a larger amount of Pd may be inducing changes in the crystalline structure and morphology of the material.

SEM analysis (Figure 3) provides morphological evidence that the presence of Pd induced the exfoliation of the MoS_2 crystal structure. The micrographs clearly show individual nanosheets and well-dispersed Pd structures (Figures 3b and 3c), indicating a breakdown of the layered stacking. This is further corroborated by XRD data (Figure 5), where the characteristic MoS_2 peak at 2θ = 14.45° exhibits a decrease in intensity, broadening, and a slight shift. These changes confirm a reduction in the crystallite size and a loss of long-range order, directly supporting the exfoliation process. The morphological changes observed are particularly significant for applications in catalysis and energy storage. In catalysis, the presence of well-dispersed Pd nanoparticles on the surface of MoS_2 is crucial, as it increases the number of available active sites, which directly enhances catalytic performance [23]. The increase in surface roughness may also provide additional sites for chemical reactions. In energy storage devices like lithium-ion batteries,

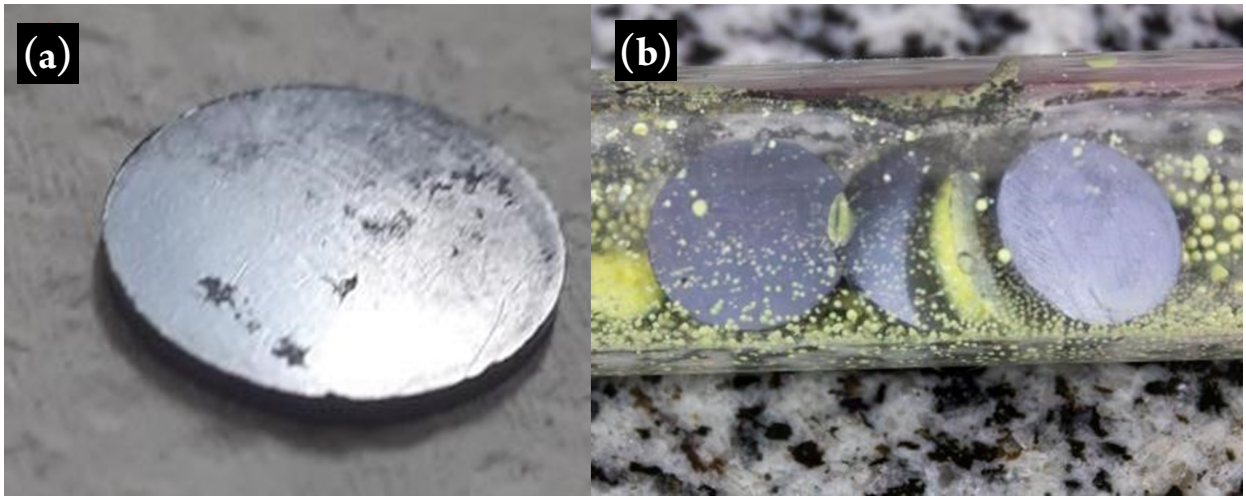

Figure 2. (a) A representative green compact specimen before heat treatment; (b) the same specimen after heat treatment.

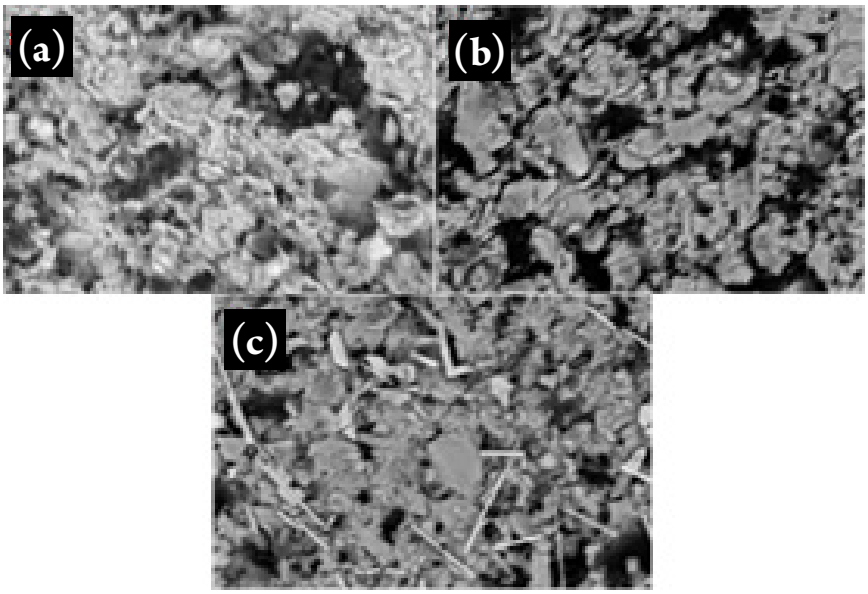

Figure 3. SEM/BSD micrographs of the samples: (a) Pure MoS_2 (b) MoS_2 with 1% Pd; and (c) MoS_2 with 2% Pd after heat treatment at 600°C.

a rougher and more fragmented morphology can facilitate ion diffusion and improve the electrochemical performance by shortening the transport path of ions and electrons [24]. The control over the morphology achieved through powder metallurgy is thus a key factor for these applications.

EDS coupled with SEM was used to map the elemental distribution in the pure MoS_2, MoS_2-1% Pd, and MoS_2-2% Pd samples. The EDS micrograph of the pure MoS_2 sample shows a uniform distribution of molybdenum (Mo) and sulfur (S), as expected. Small signs of oxygen (O) may be present, indicating slight surface oxidation. In the sample doped with 1% Pd, the elemental mapping confirms its incorporation into the MoS_2 matrix via the presence of bright spots corresponding to Pd, which appear to be relatively homogeneously distributed. With an increase to 2% Pd, the EDS mapping reveals a greater quantity of these bright spots, though some agglomeration may be present.

The EDS spectrum for pure MoS_2 (Figure 4a) shows intense peaks for Mo (Lα at ˜2.0keV and Kα at ˜17.5keV) and S (Kα at ˜2.3keV), confirming the material's composition. With the addition of 1% (Figure 4b), new peaks corresponding to Pd (Lα at ˜2.8keV) appear, confirming successful doping. For the 2% Pd sample (Figure 4c), the intensity of the Pd peaks increases significantly, as expected. Across all samples, no unexpected peaks indicating contamination were observed.

Quantitative elemental data obtained from EDS spectra are summarized in Table 2. The results show a consistent Mo:S ratio close to the stoichiometric 1:2 proportion in all samples, confirming the preservation of the MoS_2 structure after Pd doping. An in-

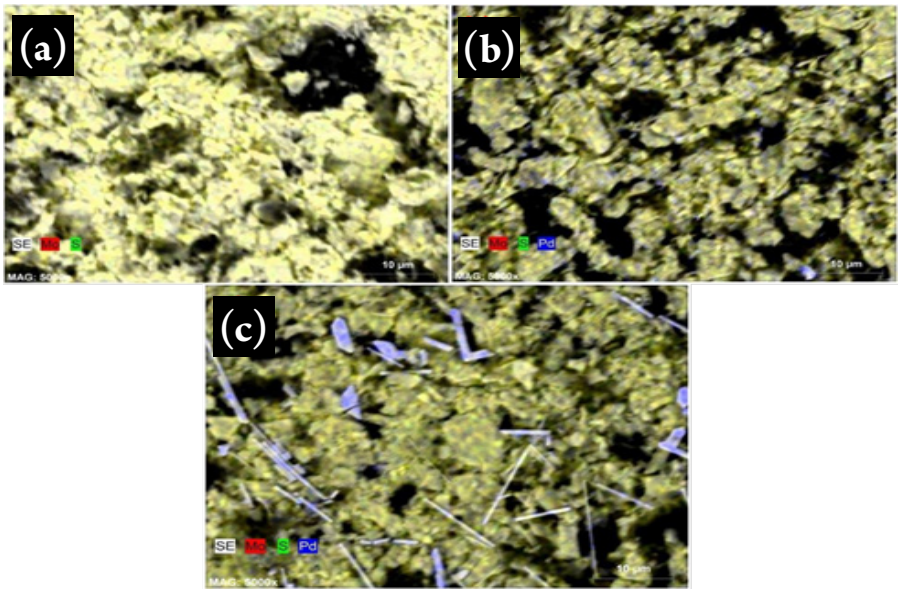

Figure 4. SEM–EDS elemental mapping of Mo, S, and Pd in (a) pure MoS_2, (b) MoS_2–1%Pd, and (c) MoS_2–2%Pd samples. The maps confirm the homogeneous distribution of Pd across the MoS_2 matrix and the preservation of the layered morphology after doping.

Table 2. Atomic and weight percentages of the elements in the MoS_2 and Pd-doped MoS_2 samples determined by EDS.

Sample	Element	Atomic %	Weight %
Pure MoS_2	Mo	30.49	56.76
	S	69.51	43.24
MoS_2 – 1% Pd	Mo	32.53	59.06
	S	67.47	40.94
	Pd	0	0
MoS_2 – 2% Pd	Mo	33.95	58.25
	S	63.13	36.20
	Pd	2.92	5.55

crease in Pd content is observed for the MoS_2–2%Pd sample, with 2.92 at.% Pd (5.55 wt.%), while Pd was below the detection limit in the MoS_2–1%Pd sample. This is expected for low doping levels, as EDS sensitivity for Pd at concentrations below ~1 at.% is limited, particularly in matrices containing heavier elements such as Mo. Despite this limitation, the compositional trend and the morphological and electrical modifications observed confirm the progressive Pd incorporation with increasing nominal content.

The X-ray diffractograms for the samples are presented in Figure 5. The analysis reveals that the characteristic peaks of hexagonal MoS_2 (indicated by red triangles) are present in all samples, confirming that the primary phase was maintained after doping and heat treatment. Peaks attributed to residual elemental sulfur (S) are also observed (blue circles).

In the pure MoS_2 sample (a), the pattern shows well-defined peaks characteristic of the 2H-MoS_2 hexagonal phase. With the introduction of 1% Pd (b), the MoS_2 peaks remain dominant but show slight changes in relative intensity, suggesting minor lattice distortions due to Pd incorporation. In the 2% Pd sample (c), the MoS_2 structure is still predominant, but there is a more expressive reduction in the peaks associated with sulfur. This suggests the increased Pd content may have facilitated a more complete sintering process. Importantly, no significant peaks corresponding to secondary palladium-containing phases (e.g., PdS) were detected in any sample, indicating that Pd was efficiently incorporated into the MoS_2 matrix, likely via substitutional doping.

The absence of secondary Pd-related peaks in the XRD patterns is a crucial finding, as it indicates the successful integration of Pd into the MoS_2 lattice without forming new, undesired phases. This is particularly important for optoelectronic and catalytic applications. For instance, the presence of separate PdS phases

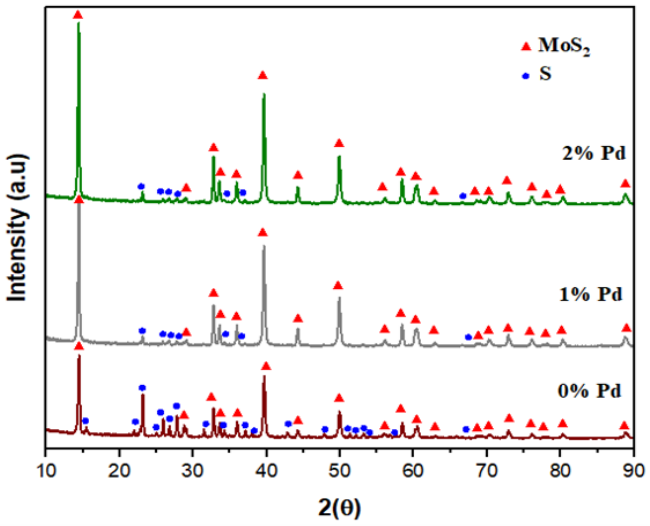

Figure 5. XRD patterns of the samples heat-treated at 600°C: (a) Pure MoS_2, (b) MoS_2-1%Pd, and (c) MoS_2-2%Pd. Red triangles denote the MoS_2 phase and blue circles denote the S phase.

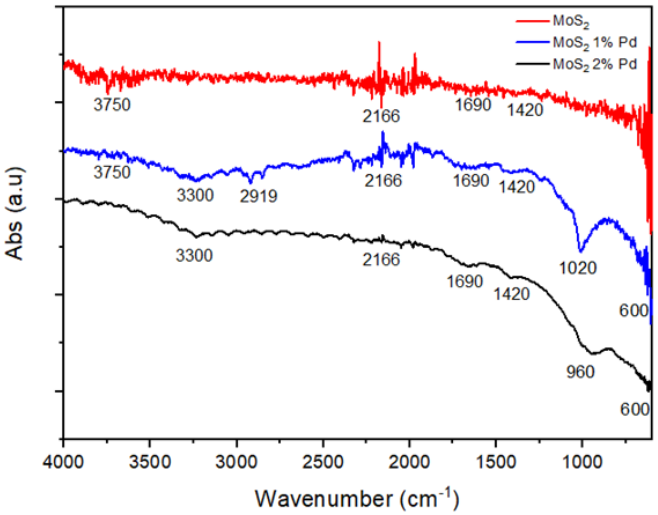

Figure 6. FTIR spectra of pure MoS_2 (red), MoS_2–1%Pd (blue), and MoS_2–2%Pd (black) samples.

could introduce new interfaces and alter the electronic band structure of the MoS_2, which is detrimental for applications in photodetectors and sensors where a precise bandgap is required [25]. The successful substitutional doping, as supported by these results, is also highly beneficial for catalysis, as it ensures that the Pd atoms are isolated or finely dispersed, acting as efficient active sites and preventing agglomeration [23].

FTIR spectroscopy was used to identify functional groups and chemical interactions [26]. The spectra for all samples are shown in Figure 6. The pure MoS_2 spectrum (red line) displays a characteristic Mo–S stretching vibration band at approximately 600cm^{-1}. Other bands at ˜1420cm^{-1}, ˜1690cm^{-1}, and ˜3750cm^{-1} suggest the presence of surface oxides or adsorbed hydroxyl groups and water [27]. Doping with 1% Pd (blue line) preserves the main MoS_2 peaks but introduces a new band at 2919cm^{-1}, possibly from C–H vibrations. With 2% Pd doping (indicated by the black line in the graphic), a new peak emerges at 960cm^{-1}, which may indicate the formation of molybdenum oxides, suggesting that a higher Pd concentration could promote surface oxidation [28]. The introduction of Pd modifies the material's surface, affecting the adsorption of functional groups [29].

The changes in the FTIR spectra, particularly the appearance of new bands with increasing Pd content, are relevant for sensing applications. The presence of surface oxides or other functional groups can create active sites that enhance the material's interaction with target gas molecules. This surface functionalization is a key strategy for improving the sensitivity and selectivity of a sensor [30]. The peak at 960cm^{-1}, potentially related to molybdenum oxides, could indicate a change in the electronic environment of the MoS_2 surface, which is a critical factor for the detection mechanism in gas sensors and photodetectors.

The appearance of the band at ~960 cm^{-1} in the FTIR spectrum of the MoS_2–2%Pd sample is attributed to the presence of oxidized molybdenum species at the surface (Mo–O stretching modes). This band does not indicate the formation of a significant amount of crystalline MoO_3, since the XRD patterns show no corresponding peaks and the EDS analyses reveal only low oxygen levels. Therefore, this oxidation is interpreted as superficial and limited, possibly related to partial sulfur loss during heating at 600°C and to a local catalytic effect of Pd, which may promote surface oxidation. Such a process can modify the bond energy and create new active sites, potentially beneficial for catalytic or sensing applications, although it may also affect stability under oxidative environments. The combined FTIR, XRD, and EDS results thus indicate that oxidation is confined to the surface and does not compromise the structural integrity of the material.

Raman spectroscopy investigates the vibrational modes of a material [30–32]. For MoS_2, the two primary Raman-active modes are the in-plane E_2g^1 mode (˜383cm^{-1}) and the out-of-plane A_1g mode (˜408cm^{-1}) [30]. The spectra for pure MoS_2 and MoS_2–2%Pd are compared in Figure 7.

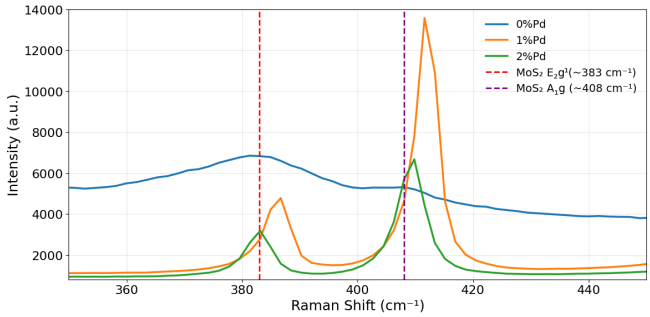

Figure 7. Raman spectra for pure MoS_2 and Pd-doped MoS_2 with 1% and 2% Pd. The graph shows a red shift and broadening of the peaks as the Pd concentration increases, indicating the interaction of the dopant with the MoS_2 crystal lattice.

Table 3. Raman Spectroscopy Parameters.

Sample	E_2g^1 (cm^{-1})	$\Delta\omega(E_2g^1)$ (cm^{-1})	A_1g (cm^{-1})	$\Delta\omega(A_1g)$ (cm^{-1})
Pure MoS_2	385.8	–	410.8	–
MoS_2 – 1% Pd	354.9	-0.9	409.6	-1.2
MoS_2 – 2% Pd	384.1	-1.7	59.06	-2.1

The pure MoS_2 spectrum (red line) shows two sharp primary peaks at 385.8 cm^{-1} (E_2g^1) and 410.8 cm^{-1} (A_1g), characteristic of a well-defined crystalline structure. In the 2% Pd doped sample (black line), the overall signal intensity is reduced, which may indicate a decrease in crystallinity or the introduction of disorder. Notably, the relative intensity of the A_1g mode increases compared to the E_2g^1 mode. This enhancement of the out-of-plane mode may be related to interactions between the Pd dopant atoms and the sulfur atoms, which would directly affect vibrations perpendicular to the basal plane.

Quantitative analysis of the Raman peaks was performed to evaluate the effect of Pd incorporation on the vibrational behavior of MoS_2. The extracted parameters are summarized in Table 3, which lists the peak positions and corresponding shifts ($\Delta\omega$) for the E_2g^1 and A_1g modes. The E_2g^1 mode shifted from 385.8 cm^{-1} in pure MoS_2 to 384.1 cm^{-1} for the 2% Pd-doped sample ($\Delta\omega$ = –1.7 cm^{-1}),

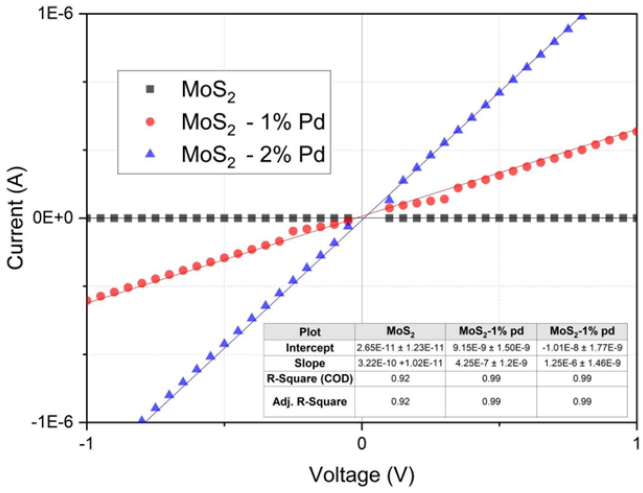

Figure 8. I-V curves for the samples: (a) Pure MoS_2 (b) MoS_2 with 1% Pd; (c) MoS_2 with 2% Pd.

while the A_1g mode moved from 410.8 to 408.7 cm^{-1} ($\Delta\omega = -2.1$ cm^{-1}). Both peaks also exhibit an increase in full width at half maximum (FWHM), indicating enhanced lattice disorder and local strain induced by Pd atoms. These quantitative results confirm the occurrence of a red shift and spectral broadening consistent with Pd–S interactions and lattice distortion within the MoS_2 structure.

The observed changes in the Raman spectra due to Pd doping provide valuable understanding into the material's structural changes. The decrease in signal intensity and the shift in the A_1g mode suggest the introduction of lattice defects or a change in the interlayer coupling, which can be beneficial for various applications. For instance, defects created by doping can act as active sites for adsorption and chemical reactions, which is a fundamental principle for highly sensitive gas sensors and catalysts [23, 30]. The modification of the interlayer interactions, as indicated by the change in the A_1g peak, could also affect the electronic band structure, a key property for optoelectronics. Therefore, the Raman analysis confirms that the dopant successfully modifies the intrinsic properties of the material, opening up possibilities for these new applications.

3.2. Electric Characterization. Electrical resistivity (ρ) was determined using two complementary techniques: I–V curve analysis and the four-point probe method. Both approaches were employed to ensure consistency and methodological rigor; however, only the I–V results are presented here for clarity, as they provided reproducible values and identical conductivity trends.

V curves (Figure 8) reveal the electrical behavior of the samples. The pure MoS_2 sample (a) exhibits characteristic non-linear, semiconducting behavior with low current in the nanoampere range. This high resistivity is expected for pristine MoS_2 and results from a low charge carrier concentration and poor electrical contacts [25]. Doping with 1% Pd (b) increases the current by nearly three orders of magnitude to the microampere range and results in a more symmetric, ohmic-like response, indicating that Pd doping effectively introduces charge carriers and improves conductivity (σ). Increasing the doping to 2% Pd (c) further enhances the current, confirming the same trend.

Table 4. Geometric parameters and calculated electrical properties for the pure and Pd-doped MoS_2 specimens.

Parameter	Sample Composition		
	Pure MoS_2	MoS_2 -1% Pd	MoS_2 -1% Pd
Radius (r) [m]	0.0027	0.0027	0.0027
Thickness (L) [m]	0.00135	0.001	0.002
Area (A) [m2]	1.539×10^{-4}	3.85×10^{-5}	1.538×10^{-4}
R [Ω]	$9.11(7) \times 10^{8}$	$1.59(4) \times 10^{6}$	$6.76(5) \times 10^{-4}$
ρ [Ωm]	$1.04(8) \times 10^{8}$	$6.14(9) \times 10^{4}$	$5.20(4) \times 10^{4}$

Comparable conductivity enhancements have been reported to significantly impact device performance. For instance, Kaushik et al. [25] demonstrated that Pd contacts to MoS_2 substantially reduced the Schottky barrier height, resulting in nearly tenfold higher current response in MoS_2-based sensors, evidencing improved charge injection and detection sensitivity. Similarly, recent studies on hybrid MoS_2/Pd catalytic structures have shown remarkable electrocatalytic performance.

The RGO/MoS_2/Pd heterostructure reported by Pandey et al. [31] exhibited an overpotential of approximately 245 mV and a Tafel slope of 42 mV·dec^{-1} for the oxygen evolution reaction (OER), indicating highly efficient charge transfer at the doped interface. In the context of energy storage, Hu et al. [24] demonstrated that incorporating conductive polymers into MoS_2, such as polyaniline (PANI), increased the specific capacitance from 150 F·g^{-1} to over 400 F·g^{-1}, while other MoS_2–carbon composites achieved values exceeding 1000 F·g^{-1} [32]. These literature benchmarks confirm that the three-order-of-magnitude increase in conductivity observed in our Pd-doped MoS_2 samples can directly translate into enhanced sensor sensitivity, catalytic efficiency, and charge storage capability, supporting the material's potential for multifunctional energy and sensing devices.

The resistivity ρ was calculated from the resistance R, obtained as the inverse slope of the linear fit of the I–V data (Figure 8), using the sample's cross-sectional area (A) and thickness (L) according to the relation $\rho = R \cdot (A/L)$. The calculated parameters are summarized in Table 4.

The conductivity increased from 9.6×10^{-9} S·m^{-1} for pure MoS_2 to 1.6×10^{-5} S·m^{-1} and 1.9×10^{-5} S·m^{-1} for the 1% and 2% Pd-doped samples, respectively, representing a three-order-of-magnitude enhancement. This trend was verified by four-point probe measurements (not shown), which yielded results within the same order of magnitude, confirming that the improvement is intrinsic and not dominated by contact resistance effects.

The experimental results demonstrate that Pd doping is an effective strategy for tailoring the electrical behavior of MoS_2. The significant reduction in resistivity validates the material's potential for applications in sensors, catalysis, and energy storage devices. In gas sensing, the initially high resistivity of pristine MoS_2 limits the detection of small resistance variations upon gas adsorption. By significantly reducing the baseline resistance, Pd doping enables a stronger and more detectable electrical signal, thereby enhancing sensor sensitivity [30]. For catalytic applications, high electrical conductivity facilitates efficient charge transfer at active sites during electrochemical reactions, such as the OER, and for energy

storage systems, it ensures faster charge/discharge kinetics and reduced internal resistance [19, 23, 24].

The remarkable improvement in conductivity is primarily attributed to the electronic effects induced by Pd incorporation within the MoS_2 lattice. The experimental evidence suggests that Pd atoms substitute Mo sites through substitutional doping, introducing shallow donor states near the conduction band that increase carrier density and mobility. This substitution also causes local lattice distortions and defect formation, as supported by the Raman red shift and peak broadening, which enhance electron–phonon coupling and interlayer transport. Additionally, Pd–S bond formation reduces the Schottky barrier height at grain boundaries and promotes charge delocalization. Collectively, these effects account for the three-order-of-magnitude enhancement in electrical conductivity and confirm the strong influence of Pd doping on the electronic structure of MoS_2.

These electrical findings are consistent with the structural and vibrational analyses presented earlier. The XRD patterns revealed a slight shift of the (002) diffraction peak toward lower angles with increasing Pd content, indicating an expansion of the interlayer spacing and partial lattice distortion. Similarly, Raman spectroscopy showed a red shift and broadening of the E_2g^1 and A_1g modes, confirming the weakening of Mo–S bonds and increased defect density. Such structural modifications facilitate charge carrier delocalization and enhance interlayer charge transport, which explains the three-order-of-magnitude improvement in electrical conductivity observed in the Pd-doped samples.

The electronic mechanism underlying the conductivity enhancement can be further understood based on previous theoretical and experimental studies. Density functional theory (DFT) simulations have shown that Pd incorporation into the MoS_2 lattice introduces shallow donor states near the conduction band and reduces the Schottky barrier height at metal–semiconductor interfaces [33-35]. These effects facilitate charge carrier delocalization and increase electrical conductivity. Furthermore, transition-metal doping has been experimentally demonstrated to modulate the band structure of MoS_2 and enhance electron mobility by several orders of magnitude [36]. These findings support our interpretation that the observed three-order-of-magnitude improvement arises from Pd-induced charge transfer and band structure modulation.

4. CONCLUSION

This research successfully demonstrated the synthesis and structural characterization of palladium-doped MoS_2, confirming the effective incorporation of palladium into the molybdenum disulfide crystal matrix. XRD analysis verified the retention of the hexagonal MoS_2 phase across all samples, though modifications in material crystallinity were noted. Crucially, the absence of peaks corresponding to secondary palladium-containing phases indicated that the adopted synthesis conditions were appropriate for achieving substitutional doping. This was further corroborated by EDS analysis, which revealed a homogeneous distribution of Pd without evidence of contamination from other elements, reinforcing the efficacy of the chosen doping method. The characterization techniques collectively revealed significant changes in the material's structure and surface chemistry upon doping. SEM imaging showed notable morphological alterations, including increased surface roughness and the formation of dispersed nanoparticles, particularly in samples with higher palladium content. FTIR spectroscopy provided further insight, showing that Pd doping induces significant changes in the material's surface composition. While the persistence of characteristic Mo-S vibrational modes confirmed the preservation of the base structure, the emergence of new spectral bands evidenced the direct influence of Pd on the compound's physicochemical properties, including potential oxidation and modified surface adsorption. Raman spectroscopy also confirmed that the dopant successfully modifies the intrinsic properties of the material, which can introduce defects that act as active sites.

The electrical property measurements were in good agreement with literature values, showing a pronounced enhancement in electrical conductivity (σ) with palladium doping, indicating an improvement in charge carrier mobility. This dramatic reduction in resistivity is a key finding that validates the material's potential for applications in sensors, catalysts, and energy storage devices.

This work demonstrates that the powder metallurgy synthesis, combined with Pd doping, successfully creates a material with optimized electrical properties. However, despite the advancements in conductivity, the full potential of the material appears to be limited by microstructural factors, such as grain boundaries, structural defects, and dopant agglomeration, which were observed in the SEM imaging. These factors act as scattering centers for charge carriers, thereby limiting mobility and suggesting the need for further

ACKNOWLEDGEMENTS

The authors would like to express their gratitude for the financial support from the Minas Gerais Research Foundation (FAPEMIG), the National Council for Scientific and Technological Development (CNPq), and the Coordination for the Improvement of Higher Education Personnel (CAPES). A special thanks is also extended to the Interdisciplinary Laboratory for Characterization, Innovation and Development (LInCaDI), where the experimental work was carried out.

CREDIT AUTHOR STATEMENT

Jonas Miguel Nogueira: Methodology, Writing-Original draft preparation, Writing-Reviewing and Editing. **Adhimar Flávio Oliveira**: Supervision, Conceptualization, Investigation, Data curation, Formal analysis, Writing-Original draft preparation. **Rero Marques Rubinger**: Formal analysis, Visualization, Data curation, Formal analysis. **Celso Henrique Correa Carvalho**: Data curation, Formal analysis, Writing-Reviewing and Editing

DECLARATIONS

Conflict of interest The authors declare that they have no known competing financial interests or personal relationships that could have appeared to influence the work reported in this paper.

REFERENCES

[1] Zhou, K., Zhang, Y., Xia, Z., & Wei, W. (2016). As-prepared MoS2 quantum dot as a facile fluorescent probe for long-term tracing of live cells. Nanotechnology, 27(27), 275101. https://doi.org/10.1088/0957-4484/27/27/275101.

[2] Rai, A., Movva, H. C., Roy, A., Taneja, D., Chowdhury, S., & Banerjee, S. K. (2018). Progress in contact, doping and mobility engineering of MoS2: an atomically thin 2D semiconductor. Crystals, 8(8), 316. https://doi.org/10.3390/cryst8080316.

[3] Zhang, J., Gu, M., & Chen, X. (2023). Supercapacitors for renewable energy applications: A review. Micro and Nano Engineering, 21, 100229. https://doi.org/10.1016/j.mne.2023.100229.

[4] Liu, Y. Z., Lu, W. M., Tran, P. P., & Pham, T. A. K. (2024). Sustainable energy and semiconductors: A bibliometric investigation. Sustainability, 16(15), 6548. https://doi.org/10.3390/su16156548.

[5] Burse, S. R., Tyagaraj, H. B., Safarkhani, M., Marje, S. J., K, G. S., Al Ghaferi, A., ... & Han, Y. K. (2025). Unleashing potential: engineering advancements in two-dimensional MoS2 for improved energy applications. Advanced Composites and Hybrid Materials, 8(2), 216. https://doi.org/10.1007/s42114-025-01289-y.

[6] Rahman, M. H., Chowdhury, E. H., & Hong, S. (2021). High temperature oxidation of monolayer MoS2 and its effect on mechanical properties: A ReaxFF molecular dynamics study. Surfaces and Interfaces, 26, 101371. https://doi.org/10.1016/j.surfin.2021.101371.

[7] Hao, L. Z., Liu, Y. J., Gao, W., Liu, Y. M., Han, Z. D., Xue, Q. Z., & Zhu, J. (2016). Enhanced photovoltaic characteristics of MoS2/Si hybrid solar cells by metal Pd chemical doping. RSC Advances, 6(2), 1346-1350. https://doi.org/10.1039/c5ra24453f.

[8] Prasad, J., Singh, A. K., Gahlot, A. P. S., Tomar, M., Gupta, V., & Singh, K. (2021). Electromagnetic interference shielding properties of hierarchical core-shell palladium-doped MoS2/CNT nanohybrid materials. Ceramics International, 47(19), 27586-27597. https://doi.org/10.1016/j.ceramint.2021.06.183.

[9] Qiu, H., Yu, Z., Zhao, T., Zhang, Q., Xu, M., Li, P., Wang, X. (2024). Two-dimensional materials for future information technology: status and prospects. Science China Information Sciences, 67(6), 160400. https://doi.org/10.1007/s11432-024-4033-8.

[10] Karki, S. (2023). Structural and Electronic Properties of Palladium and Palladium Doped Graphene. Int. J. Sci. Res. in Physics and Applied Sciences Vol, 11(5).

[11] Cai, Z., Liu, B., Zou, X., & Cheng, H. M. (2018). Chemical vapor deposition growth and applications of two-dimensional materials and their heterostructures. Chemical reviews, 118(13), 6091-6133. https://doi.org/10.1021/acs.chemrev.7b00536.

[12] Acar, M., & Gür, E. (2021). Sputtered 2D transition metal dichalcogenides: from growth to device applications. Turkish Journal of Physics, 45(3), 131-147. https://doi.org/10.3906/fiz-2104-8.

[13] Danks, A. E., Hall, S. R., & Schnepp, Z. J. M. H. (2016). The evolution of 'sol–gel'chemistry as a technique for materials synthesis. Materials Horizons, 3(2), 91-112. https://doi.org/10.1039/C5MH00260E.

[14] Chiaverini, V. (1986). Tecnologia Mecânica: Volume 1: Estrutura e Propriedade das Ligas Metálicas (2a ed.). McGraw-Hill.

[15] Chiaverini, V. (1992). Metalurgia do Pó: Técnicas e Produtos (3a ed.). Edite Serviços Gráficos e Editora Ltda.

[16] Groover, M. P. (2010). Fundamentals of Modern Manufacturing: Materials, Processes and Systems (4th ed.). John Wiley & Sons.

[17] Sharma, M., Vajpai, S. K., & Dube, R. K. (2010). Processing and characterization of Cu-Al-Ni shape memory alloy strips prepared from elemental powders via a novel powder metallurgy route. Metallurgical and Materials Transactions A, 41(11), 2905-2913. https://doi.org/10.1007/s11661-010-0351-y.

[18] Upadhyaya, G. S. (1997). Powder metallurgy technology. Cambridge Int Science Publishing.

[19] Setiawan, Luo, Z., Ouyang, Y., Zhang, H., Xiao, M., Ge, J., Jiang, Z., Xing, W. (2018). Chemically activating MoS2 via spontaneous atomic palladium interfacial doping towards efficient hydrogen evolution. Nature communications, 9(1), 2120. https://doi.org/10.1038/s41467-018-04501-4.

[20] Callister Jr, W. D., & Rethwisch, D. G. (2020). Materials science and engineering: an introduction. John wiley & sons.

[21] Kittel, C., & McEuen, P. (2018). Introduction to solid state physics. John Wiley & Sons.

[22] Vikraman, H. K., George, J., Ghuge, R. S., Painappallil Reji, R., Jayaraman, S. V., Kawazoe, Y., ... & Mangalampalli, S. K. (2025). Highly Selective, Room-Temperature Triethylamine Sensor Using Humidity-Resistant Novel TiZn Alloy Nanoparticles-Decorated MoS_2 Nanosheets. Small, 21(1), 2408500. https://doi.org/10.1002/smll.202408500.

[23] Guo, M., Jin, Z., Pan, J., Xu, J., Guo, L., Yin, X. B., ... & Zhang, M. (2024). Construction of COFs@ MoS2-Pd hierarchical tubular heterostructures for enhanced catalytic performance. Inorganic chemistry, 63(39), 18263-18275. https://doi.org/10.1021/acs.inorgchem.4c03151.

[24] Hu, L., Ren, Y., Yang, H., & Xu, Q. (2014). Fabrication of 3D hierarchical MoS2/polyaniline and MoS2/C architectures for lithium-ion battery applications. ACS applied materials & interfaces, 6(16), 14644-14652. https://doi.org/10.1021/am503995s.

[25] Kaushik, N., Nipane, A., Basheer, F., Dubey, S., Grover, S., Deshmukh, M. M., & Lodha, S. (2014). Schottky barrier heights for Au and Pd contacts to MoS2. Applied Physics Letters, 105(11). https://doi.org/10.1063/1.4895767.

[26] Matthews, T., Chabalala, M. P., Mbokazi, S. P., Zikhali, M., Dolla, T. H., Šarakovskis, A., ... & Maxakato, N. W. (2025). Improving the electrocatalytic activity of Pd nanoparticles through electronic coupling interaction with a Ni 2 P–MoS 2 hybrid support for ethanol electro-oxidation in an alkaline medium. Sustainable Energy & Fuels, 9(6), 1552-1564. https://doi.org/10.1039/D4SE01223B.

[27] Wang, W., Tang, L., Chen, C., Wang, X., Wang, Y., & Sun, W. (2024). Engineering Pt–S–Mo and Pd–S–Mo sites in hier-

archical porous MoS2 for boosted oxygen reduction activity in microbial fuel cell. Journal of Power Sources, 598, 234143. https://doi.org/10.1016/j.jpowsour.2024.234143.

[28] Luo, Z., Guo, Y., He, C., Guan, Y., Zhang, L., Li, Y., ... & Ren, X. (2024). Creating High-entropy Single Atoms on Transition Disulfides through Substrate-induced Redox Dynamics for Efficient Electrocatalytic Hydrogen Evolution. Angewandte Chemie International Edition, 63(32), e202405017. https://doi.org/10.1002/anie.202405017.

[29] Quirós-Ovies, R., Bastante, P., Hettler, S., Vega-Mayoral, V., Aina, S., Balos, V., ... & Sebastian, V. (2024). Chemically-linked heterostructures of palladium nanosheets and 2H-MoS2. Small, 2406030. https://doi.org/10.1002/smll.202406030.

[30] Samy, O., Zeng, S., Birowosuto, M. D., & El Moutaouakil, A. (2021). A review on MoS2 properties, synthesis, sensing applications and challenges. Crystals, 11(4), 355. https://doi.org/10.3390/cryst11040355.

[31] Pandey, A., Mukherjee, A., Chakrabarty, S., Chanda, D., & Basu, S. (2019). Interface engineering of an RGO/MoS2/Pd 2D heterostructure for electrocatalytic overall water splitting in alkaline medium. ACS applied materials & interfaces, 11(45), 42094-42103. https://doi.org/10.1021/acsami.9b13358.

[32] Tang, Z., Dai, J., Wei, W., Gao, Z., Liang, Z., Wu, C., ... & Dai, L. (2022). In situ generation of ultrathin MoS2 nanosheets in carbon matrix for high energy density photo-responsive supercapacitors. Advanced Science, 9(24), 2201685. https://doi.org/10.1002/advs.202201685.

[33] Cai, Y., Zhou, H., Zhang, G., & Zhang, Y. W. (2016). Modulating carrier density and transport properties of MoS2 by organic molecular doping and defect engineering. Chemistry of Materials, 28(23), 8611-8621. https://doi.org/10.1021/acs.chemmater.6b03539.

[34] Kim, G. S., Kim, S. H., Park, J., Han, K. H., Kim, J., & Yu, H. Y. (2018). Schottky barrier height engineering for electrical contacts of multilayered MoS2 transistors with reduction of metal-induced gap states. ACS nano, 12(6), 6292-6300. https://doi.org/10.1021/acsnano.8b03331.

[35] Urquiza, M. L., & Cartoixà, X. (2020). Schottky barriers, emission regimes and contact resistances in 2H-1T'MoS2 lateral metal-semiconductor junctions from first-principles. 2D Materials, 7(4), 045030. https://doi.org/10.1088/2053-1583/aba449.

[36] Ma, D., Ju, W., Li, T., Zhang, X., He, C., Ma, B., ... & Yang, Z. (2016). Modulating electronic, magnetic and chemical properties of MoS2 monolayer sheets by substitutional doping with transition metals. Applied Surface Science, 364, 181-189. https://doi.org/10.1016/j.apsusc.2015.12.142.